OPEN ACCESS
Unmanned Systems (2025)

DOI: 10.1142/S2301385025500190

UNMANNED SYSTEMS
https://www.worldscientific.com/worldscinet/us

Design and Control of an Innovative Overactuated Thrust Vectoring Six-DoF Quadrotor for Extreme and Challenging Environments

Mohamed Kara-Mohamed *,‡, Qian Zhang *, Xinggang Yan †

*The School of Engineering, Liverpool John Moores University Tithebarn Street, Liverpool L2 2QP, UK

†School of Engineering University of Kent, Canterbury, Kent CT2 7NT, UK

The wide spectrum of recent applications for UAVs imposes further challenges to their abilities and control. This is especially true when operating in harsh and hostile environments where disturbances are huge and actuators are prone to failure. Conventional systems and traditional control techniques are not sufficient for stability and tracking under these circumstances. This paper proposes a unique innovative overactuated quadrotor system that has six DoFs. The vehicle has four rotors and each rotor can tilt independently in the *YZ*-plane. It has the ability to correct its position and attitude in a decoupled way which is different from the conventional quadrotor configurations. Sliding-mode control associated with switching control mode is used for the control algorithm of the system. The system shows agility in the face of large disturbances and robustness against actuator failure which makes it a perfect fit for extreme and challenging environments. The concept of the system and its ability are illustrated in simulation with promising results.

Keywords: UAVs; sliding-mode control; switching control; quadrotor; thrust vectoring.

US

1. Introduction

Unmanned Aerial Vehicles (UAVs) have recently gained significant research and commercial attention. They have been deployed in a wide spectrum of civil applications including remote operations, lifting, sensing and communications [1–3]. Quadrotor is a common class of UAVs that is widely used due to its symmetry, which is an advantage for maneuverability, stability and control [4–6].

The wide deployment of UAVs in extended range of applications challenges their ability to fly in various environments and weather conditions. In the context of UAV operation, extreme conditions and challenging environments are usually associated with factors that seriously affect the UAV performance such as huge disturbances resulting from strong wind, heavy rain and unpredictable weather conditions [7] or the ingress of small particles in the atmosphere from dusts, icing, sea-salt and pollution which might lead to actuator and sensor failure [8, 9]. This necessitates development in the control techniques and aerodynamic design to enable UAVs to work under extreme conditions and challenging environments. This challenge for operating a UAV in severe conditions has been investigated by several researchers (see e.g. [10, 11] and the references therein). To overcome these challenges, the focus is usually either on developing a robust control algorithm that can stabilize the system and ensure good tracking in the presence of these disturbances or on developing a specific system design configuration that increases the ability of the system to respond to and reject the disturbances [12–14].

From the configuration and design perspective, UAVs have seen various developments related to the configuration of the rotors and the airframe design. The main aim of the research in this direction is to enhance the maneuverability and stability of the vehicle, see, for instance, [15–18]. One of the main techniques that is used to enhance

Received 14 July 2023; Revised 5 October 2023; Accepted 31 October 2023; Published 14 November 2023. This paper was recommended for publication in its revised form by editorial board member, Wen-Hua Chen.
Email Address: ‡*m.karamohamed@ljmu.ac.uk*
‡Corresponding author.

the performance of UAVs is thrust vectoring [19, 20]. It is used in various UAV configurations including quadrotors. It can be achieved by simply tilting the thrust generating system (the rotors) or designing the system with fixed tilted nonplanar rotors [21–23]. Thrust vectoring technology overcomes the intrinsic limitations of conventional standard coplanar architecture [24]. It enables the system to generate forces and torques in six-degree-of-freedom (DoF) envelope which extends the ability of the vehicle to fly in any direction while maintaining any arbitrary orientation [23, 25]. On the other hand, thrust vectoring for quadrotors creates overactuated systems with more complex and nonlinear control problem. This issue has been addressed explicitly in [26] using pseudo-inverse matrices and by solving a complementary optimization problem, while in [27], thrust–tilting angle limitations are taken into account with prioritization of the position and attitude to solve the overactuation nonlinear control problem.

From the control development perspective, the control of UAV systems is well established in the literature with both linear and nonlinear control techniques [6, 28–30]. Sliding-mode control (SMC) is a nonlinear control tool that is based on Lyapunov stability criteria. It is suitable for quadrotor control due to its advantages of insensitivity to modeling error, parametric uncertainties and other disturbances [6, 31, 32]. This robustness feature of sliding-mode control has been utilized to enhance the UAVs' operations against uncertainties and external disturbances [12, 33, 34], where the sliding-mode control has been used for UAVs of conventional configuration with promising results [14, 35, 36]. For instance, in [37], the authors showed how an adaptive backstepping global sliding-mode control can be used for quadrotors to stabilize the system and ensure finite-time tracking in the presence of input saturation, model uncertainty and wind perturbation. In [38], it was shown that an adaptive PID-sliding-mode control can be used to overcome external disturbances and sensor failure. However, SMC suffers from a chattering phenomenon that affects the controller performance. Several methods and techniques have been proposed in the literature to minimize the chattering effect when utilizing SMC, see e.g. [39–41].

On the other hand, switching control strategy has been used by several projects in the control design of UAVs [42, 43]. Switching-mode scheme depends on mapping the dynamics of the UAV into a set of finite modes in order to improve the efficiency of the controller and overcome various control and computational challenges [44].

This paper approaches the problem of UAVs' flight in hostile environments from both perspectives: the UAV configuration and the control synthesis. The main contribution of the paper is the proposal of an innovative overactuated thrust vectoring six-degree-of-freedom (DOF) quadrotor which is controlled using an MIMO sliding mode associated with the switching control technique. The ability of the system to overcome large disturbances and tolerate actuator failure is shown in simulation. The proposed system does not exist in the literature and the use of sliding-mode control along with switching-mode technique for such a system has not been reported in published research before.

The designed quadrotor overcomes the well-known inherited disadvantages of underactuated quadrotor systems. The proposed overactuated system with the designed controller enables the vehicle to achieve a decoupled position and orientation trajectory tracking, without prioritization or restricted flight envelope, as well as reject large disturbances and withstand faulty actuators. This is an important and useful advantage especially in harsh and difficult applications which is the main target for the development of this system. The purpose of this paper is to demonstrate the ability of the proposed systems and associated controller and not to compare the performance of the controller with other established techniques, and hence the paper does not contain any comparative analysis between the proposed controller and other controllers.

The configuration of the proposed system is presented in Sec. 2. The dynamic model is derived in Sec. 3 and the control synthesis is introduced in Sec. 4. The simulation study is then detailed in Sec. 5 and the paper concludes with some remarks and conclusions in Sec. 6.

2. System Configuration

The proposed system is shown in Fig. 1. It is a symmetrical cross-quadrotor of length l for each arm with four identical rotors as displayed in Fig. 2. We assume the rotors are spinning by independent highly efficient brushless DC (BLDC) motors. Each opposite pair of rotors rotates in the opposite direction to eliminate the counteracting torque. We randomly select rotors 1 and 3 to rotate in the anti-clockwise direction, while rotors 2 and 4 rotate clockwise, see Fig. 2. Each rotor can be tilted independently in the

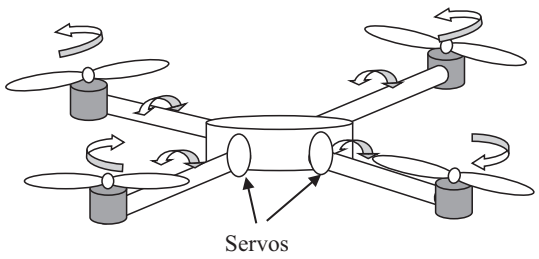

Fig. 1. The design of the proposed six-DoF UAV (3D view).

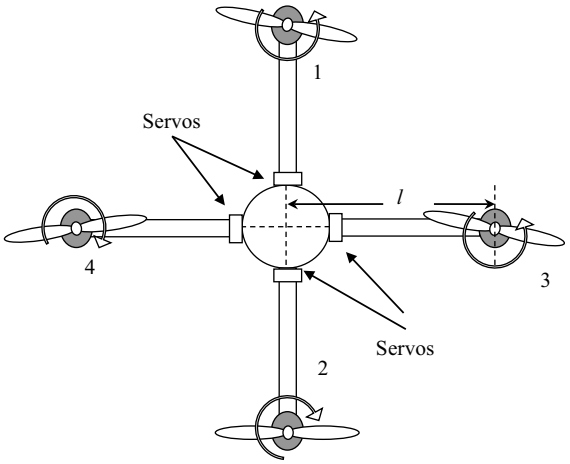

Fig. 2. Top view of the proposed quadrotor.

YZ-plane by an angle α_i within the range $\left[-\frac{\pi}{2}, \frac{\pi}{2}\right]$, see Figs. 3 and 4, using a servo motor that is fixed at the mount of the brushless DC motor. The tilting angle is positive in the clockwise direction along the positive direction of the *Y*-axis as shown in Fig. 3.

3. Modeling and Control

The model of the proposed quadrotor is derived using the Euler angles notation and Newton's Second Law. To derive the mathematical model of the system, we use the right-hand coordinate frames shown in Fig. 4. Frame *e* represents the earth fixed coordinates and frame *b* represents the body coordinates that coincide with the center of gravity of the

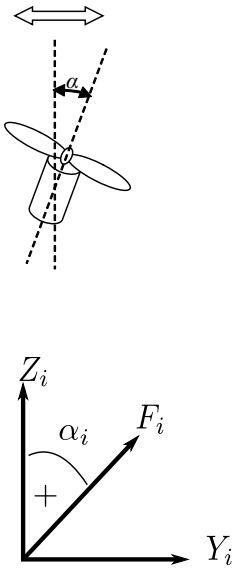

Fig. 3. The thrust vectoring tilting angle.

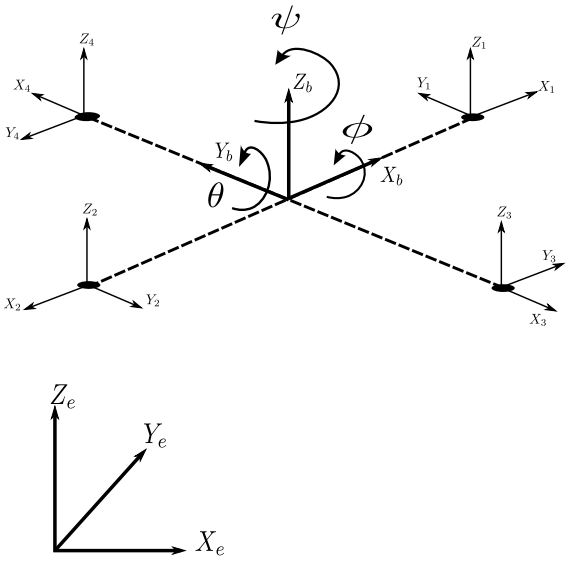

Fig. 4. Frames of the quadrotor system.

UAV. In addition, we use local coordinate frames that are fixed at the center point of each rotor as shown in Fig. 4.

The rotation matrix from the earth frame *e* to the body frame *b*, using the conventional attitude angles Yaw ψ, Pitch θ and Roll ϕ, as shown in Fig. 4, with the sequence *ZYX*, is given by

$$R_e^b = \begin{bmatrix} C_\theta C_\psi & C_\theta S_\psi & -S_\theta \\ -C_\phi S_\psi + S_\phi S_\theta C_\psi & C_\phi C_\psi + S_\phi S_\theta S_\psi & S_\phi C_\theta \\ S_\phi S_\psi + C_\phi S_\theta C_\psi & -S_\phi C_\psi + C_\phi S_\theta S_\psi & C_\phi C_\theta \end{bmatrix}, \tag{1}$$

where $C_\cdot = \cos(\cdot)$ and $S_\cdot = \sin(\cdot)$.

Following the general notion of rotation matrices, the rotation matrices from the local coordinates of the rotors to the body coordinate of the quadrotor *b* can be derived as

$$R_1^b = \begin{bmatrix} 1 & 0 & 0 \\ 0 & 1 & 0 \\ 0 & 0 & 1 \end{bmatrix}, \quad R_2^b = \begin{bmatrix} -1 & 0 & 0 \\ 0 & -1 & 0 \\ 0 & 0 & 1 \end{bmatrix},$$
$$R_3^b = \begin{bmatrix} 0 & 1 & 0 \\ -1 & 0 & 0 \\ 0 & 0 & 1 \end{bmatrix}, \quad R_4^b = \begin{bmatrix} 0 & -1 & 0 \\ 1 & 0 & 0 \\ 0 & 0 & 1 \end{bmatrix}. \tag{2}$$

The forces acting on the system are the propulsive force and gravity force. The Cartesian components of the individual propulsive force from each rotor expressed in the local coordinates are

$$F_i = \begin{bmatrix} 0 \\ k_f \omega_i^2 \sin \alpha_i \\ k_f \omega_i^2 \cos \alpha_i \end{bmatrix}, \tag{3}$$

with $i = 1, 2, 3, 4$. The term k_f is the thrust constant of the propulsion system which depends on the rotor blade characteristics, the air density and the thrust coefficient of the propeller. The rotational speed of each rotor is ω_i and α_i is the tilting angle as defined in Fig. 3.

The propulsive force in the body frame is

$$F_i^b = R_i^b F_i, \tag{4}$$

which gives

$$F_1^b = \begin{bmatrix} 0 \\ k_f\omega_1^2 \sin\alpha_1 \\ k_f\omega_1^2 \cos\alpha_1 \end{bmatrix}, \quad F_2^b = \begin{bmatrix} 0 \\ -k_f\omega_2^2 \sin\alpha_2 \\ k_f\omega_2^2 \cos\alpha_2 \end{bmatrix},$$
$$F_3^b = \begin{bmatrix} k_f\omega_3^2 \sin\alpha_3 \\ 0 \\ k_f\omega_3^2 \cos\alpha_3 \end{bmatrix}, \quad F_4^b = \begin{bmatrix} -k_f\omega_4^2 \sin\alpha_4 \\ 0 \\ k_f\omega_4^2 \cos\alpha_4 \end{bmatrix}. \tag{5}$$

The total propulsive force in the body frame is

$$F_p^b = \Sigma F_i^b \tag{6}$$
$$= k_f H_1 U, \tag{7}$$

with

$$H_1 = \begin{bmatrix} 0 & 0 & 0 & 0 & 1 & 0 & -1 & 0 \\ 1 & 0 & -1 & 0 & 0 & 0 & 0 & 0 \\ 0 & 1 & 0 & 1 & 0 & 1 & 0 & 1 \end{bmatrix} \tag{8}$$

and

$$U = \begin{bmatrix} \omega_1^2 \sin\alpha_1 \\ \omega_1^2 \cos\alpha_1 \\ \omega_2^2 \sin\alpha_2 \\ \omega_2^2 \cos\alpha_2 \\ \omega_3^2 \sin\alpha_3 \\ \omega_3^2 \cos\alpha_3 \\ \omega_4^2 \sin\alpha_4 \\ \omega_4^2 \cos\alpha_4 \end{bmatrix}. \tag{9}$$

The gravity force in the body frame is given by

$$F_g^b = R_e^b \begin{bmatrix} 0 \\ 0 \\ mg \end{bmatrix} \tag{10}$$
$$= mgR_g, \tag{11}$$

with

$$R_g = \begin{bmatrix} -S_\theta \\ S_\phi C_\theta \\ C_\phi C_\theta \end{bmatrix}, \tag{12}$$

where m is the total weight of the UAV and g is the gravity acceleration constant.

The total force acting on the UAV becomes

$$F_\Sigma = k_f H_1 U + mgR_g. \tag{13}$$

Two main torques affect the quadrotor which are the propulsive torque resulting from the propulsion force and the drag torque.

The individual propulsive torque from each rotor around the center of gravity can be given as

$$T_{p_i}^b = l_i^b \times F_i^b, \tag{14}$$

where

$$l_i^b = R_i^b \begin{bmatrix} l \\ 0 \\ 0 \end{bmatrix}. \tag{15}$$

This leads to

$$T_{p_1}^b = \begin{bmatrix} 0 \\ -lk_f\omega_1^2 \cos\alpha_1 \\ lk_f\omega_1^2 \sin\alpha_1 \end{bmatrix}, \quad T_{p_2}^b = \begin{bmatrix} 0 \\ lk_f\omega_2^2 \cos\alpha_2 \\ lk_f\omega_2^2 \sin\alpha_2 \end{bmatrix},$$
$$T_{p_3}^b = \begin{bmatrix} -lk_f\omega_3^2 \cos\alpha_3 \\ 0 \\ lk_f\omega_3^2 \sin\alpha_3 \end{bmatrix}, \quad T_{p_4}^b = \begin{bmatrix} lk_f\omega_4^2 \cos\alpha_4 \\ 0 \\ lk_f\omega_4^2 \sin\alpha_4 \end{bmatrix}. \tag{16}$$

The total propulsive torque in the body frame is

$$T_p^b = \Sigma T_{p_i}^b \tag{17}$$
$$= lk_f H_2 U, \tag{18}$$

with

$$H_2 = \begin{bmatrix} 0 & 0 & 0 & 0 & 0 & -1 & 0 & 1 \\ 0 & -1 & 0 & 1 & 0 & 0 & 0 & 0 \\ 1 & 0 & 1 & 0 & 1 & 0 & 1 & 0 \end{bmatrix} \tag{19}$$

and U being defined as in Eq. (9).

The individual drag torque resulting from the rotation of each propeller acts in the opposite direction to that of rotation and can be derived in the form of a scalar value as

$$T_{d_i} = -k_d\omega_i^2, \tag{20}$$

where k_d is the drag constant that is related to the propeller design and the flight environment. The negative sign indicates that the torque is in opposite direction to that of rotation.

Similar to the propulsive force analysis, the drag torques in the body coordinate system are given by

$$T_{d_i}^b = R_i^b T_{d_i}, \tag{21}$$

which gives

$$T_{d_1}^b = \begin{bmatrix} 0 \\ -k_d\omega_1^2 \sin\alpha_1 \\ -k_d\omega_1^2 \cos\alpha_1 \end{bmatrix}, \quad T_{d_2}^b = \begin{bmatrix} 0 \\ -k_d\omega_2^2 \sin\alpha_2 \\ k_d\omega_2^2 \cos\alpha_2 \end{bmatrix},$$
$$T_{d_3}^b = \begin{bmatrix} -k_d\omega_3^2 \sin\alpha_3 \\ 0 \\ -k_d\omega_3^2 \cos\alpha_3 \end{bmatrix}, \quad T_{d_4}^b = \begin{bmatrix} -k_d\omega_4^2 \sin\alpha_4 \\ 0 \\ k_d\omega_4^2 \cos\alpha_4 \end{bmatrix}. \tag{22}$$

The total drag torque in the body frame can be expressed as

$$T_d^b = \Sigma T_{d_i}^b \tag{23}$$

$$= k_d H_3 U, \tag{24}$$

with

$$H_3 = \begin{bmatrix} 0 & 0 & 0 & 0 & -1 & 0 & -1 & 0 \\ -1 & 0 & -1 & 0 & 0 & 0 & 0 & 0 \\ 0 & -1 & 0 & 1 & 0 & -1 & 0 & 1 \end{bmatrix} \tag{25}$$

and U being defined as in Eq. (9).

The total torque working on the system is

$$T_\Sigma = (lk_f H_2 + k_d H_3)U \tag{26}$$

$$= H_4 U, \tag{27}$$

with

$$H_4 = \begin{bmatrix} 0 & 0 & 0 & 0 & -k_d & -lk_f & -k_d & lk_f \\ -k_d & -lk_f & -k_d & lk_f & 0 & 0 & 0 & 0 \\ lk_f & -k_d & lk_f & k_d & lk_f & -k_d & lk_f & k_d \end{bmatrix}. \tag{28}$$

In the above analysis of the total forces and torques affecting the system, the gyroscopic force and the gyroscopic inertia are ignored and assumed to be negligible. The gyroscopic effect results from the tilting of the spinning propellers. It is assumed that this effect can be ignored safely in the modeling process by considering it as second-order disturbances to be rejected by the controller. This assumption is valid as long as the inertia of the propeller is very small compared to the inertia of main body of the vehicle.

Following standard Newton–Euler equations in the body frame, the dynamic model of the system is

$$F_\Sigma = m(\dot{\varepsilon} + \zeta \times \varepsilon), \tag{29}$$

$$T_\Sigma = I\dot{\zeta} + \zeta \times (I\zeta). \tag{30}$$

The term I represents the inertia matrix of the UAV with respect to the fixed body coordinate system. Assuming even distribution of mass across the body of the UAV and given that the vehicle is symmetric, the inertial matrix I is diagonal with the components of I_{xx}, I_{yy} and I_{zz} only. The terms ε and ζ represent the translational and rotational velocities of the UAV. In the body frame, the components of these velocities are given by

$$\varepsilon = \begin{bmatrix} u \\ v \\ w \end{bmatrix}, \quad \zeta = \begin{bmatrix} p \\ q \\ r \end{bmatrix}. \tag{31}$$

Substituting the forces and torques into Eqs. (29) and (30) gives the dynamic model of the quadrotor as

$$\dot{\varepsilon} = gR_g - W\varepsilon + k_t H_1 U, \tag{32}$$

$$\dot{\zeta} = I^{-1}H_4 U - I^{-1}W(I\zeta), \tag{33}$$

where the constant $k_t = \frac{k_f}{m}$ and the matrix W is the skew matrix of the angular velocity which is given by

$$W = \begin{bmatrix} 0 & -r & q \\ r & 0 & -p \\ -q & p & 0 \end{bmatrix}. \tag{34}$$

Using the standard notation of rotational matrices between frames, the absolute position and orientation of the vehicle defined in the earth coordinate system as a function of the measured translational and rotational speeds in the body frame can be obtained as

$$\dot{Y}_1 = R_b^e \varepsilon, \tag{35}$$

$$\dot{Y}_2 = \Psi\zeta, \tag{36}$$

with $R_b^e = (R_e^b)^{-1} = (R_e^b)^T$ and

$$Y_1 = \begin{bmatrix} x \\ y \\ z \end{bmatrix}, \quad Y_2 = \begin{bmatrix} \phi \\ \theta \\ \psi \end{bmatrix},$$
$$\Psi = \begin{bmatrix} 1 & S_\phi S_\theta / C_\theta & C_\phi S_\theta / C_\theta \\ 0 & C_\phi & -S_\phi \\ 0 & S_\phi / C_\theta & C_\phi / C_\theta \end{bmatrix}. \tag{37}$$

Assuming that the output of the system is $Y = [Y_1, Y_2]^T = [x\ y\ z\ \phi\ \theta\ \psi]^T$, and the input vector U is as defined in Eq. (9), the model in Eqs. (32) and (33) with

Eqs. (35) and (36) shows a state space representation of nonlinear overactuated system that has six outputs and eight inputs. This redundancy represents the merits of the proposed quadrotor where it decouples the position and attitude of the vehicle to give better maneuverability and more disturbance rejection. However, at the same time, it imposes a control challenge that will be addressed in the next section.

The dynamic model of the system can be made square by expanding Eqs. (32) and (33) and introducing a new input as

$$\bar{U} = \begin{bmatrix} \bar{U}_1 \\ \bar{U}_2 \end{bmatrix}, \tag{38}$$

with

$$\bar{U}_1 = \begin{bmatrix} U_u \\ U_v \\ U_w \end{bmatrix}, \qquad \bar{U}_2 = \begin{bmatrix} U_p \\ U_q \\ U_r \end{bmatrix}, \tag{39}$$

where

$$\bar{U}_u = k_t(\omega_3^2 \sin\alpha_3 - \omega_4^2 \sin\alpha_4), \tag{40}$$

$$\bar{U}_v = k_t(\omega_1^2 \sin\alpha_1 - \omega_2^2 \sin\alpha_2), \tag{41}$$

$$\bar{U}_w = k_t(\omega_1^2 \cos\alpha_1 + \omega_2^2 \cos\alpha_2 + \omega_3^2 \cos\alpha_3 + \omega_4^2 \cos\alpha_4), \tag{42}$$

$$\bar{U}_p = (lk_f / I_{xx})(\omega_4^2 \cos\alpha_4 - \omega_3^2 \cos\alpha_3) - (k_d / I_{xx}) \times (\omega_3^2 \sin\alpha_3 + \omega_4^2 \sin\alpha_4), \tag{43}$$

$$\bar{U}_q = (lk_f / I_{yy})(\omega_2^2 \cos\alpha_2 - \omega_1^2 \cos\alpha_1) - (k_d / I_{yy}) \times (\omega_1^2 \sin\alpha_1 + \omega_2^2 \sin\alpha_2), \tag{44}$$

$$\bar{U}_r = (lk_f / I_{zz})(\omega_1^2 \sin\alpha_1 + \omega_2^2 \sin\alpha_2 + \omega_3^2 \sin\alpha_3 + \omega_4^2 \sin\alpha_4) \tag{45}$$

$$+ (k_d / I_{zz})(-\omega_1^2 \cos\alpha_1 + \omega_2^2 \cos\alpha_2 - \omega_3^2 \cos\alpha_3 + \omega_4^2 \cos\alpha_4), \tag{46}$$

which means the system model can be written in compact matrix form as

$$\dot{\varepsilon} = N_1 + \bar{U}_1, \tag{47}$$

$$\dot{\zeta} = N_2 + \bar{U}_2, \tag{48}$$

$$\dot{Y}_1 = R_b^e \varepsilon, \tag{49}$$

$$\dot{Y}_2 = \Psi \zeta, \tag{50}$$

where

$$N_1 = \begin{bmatrix} -gS_\theta - (qw - rv) \\ gS_\phi C_\theta - (ur - pw) \\ gC_\phi C_\theta - (pv - qu) \end{bmatrix}, \qquad N_2 = \begin{bmatrix} I_p qr \\ I_q rp \\ I_r pq \end{bmatrix}, \tag{51}$$

and

$$I_p = \frac{I_{zz} - I_{yy}}{I_{xx}}, \tag{52}$$

$$I_q = \frac{I_{xx} - I_{zz}}{I_{yy}}, \tag{53}$$

$$I_r = \frac{I_{yy} - I_{xx}}{I_{zz}}. \tag{54}$$

This representation makes the dynamic model of the system square having six outputs, the vector Y, and six inputs, the virtual input vector $\bar{U}$, however, the number of physical actuators of the system is eight and hence the system is still overactuated between its real actuators and the required outputs. The full control synthesis of the system will be discussed in detail in the following section.

4. Control Synthesis

The controller of the proposed overactuated quadrotor is designed for the tracking problem which involves two steps. In the first step, it needs to find the required virtual input vector $\bar{U}$ to drive the system to the desired position and orientation. The second step is to transform the virtual input vector into the physical quantities of motor angular

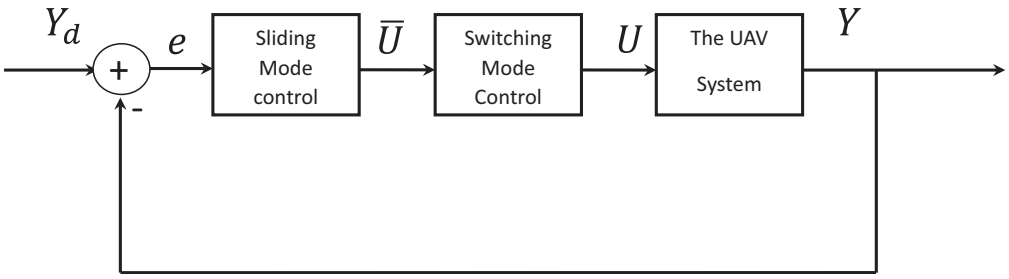

Fig. 5. The block diagram of the control system.

speed and servo tilting angles using Eqs. (40)–(46). We address the first step of the control problem using sliding-mode control algorithm while the determination of the motor angular speeds and servo tilting angles will be made using a switching-mode algorithm. These two steps are shown in the block diagram in Fig. 5 and will be detailed in the following subsections. In this figure, Y_d is the desired output target, e is the error between the actual output of the system and the desired output and $\bar{U}$ and U are the virtual input and the actual input of the system as defined before in Eqs. (38) and (9) subsequently.

4.1. *The relative degree of the system*

To design a sliding-mode control, we need to determine the relative degree of the system. Assuming that

$$Y = \begin{bmatrix} Y_1 \\ Y_2 \end{bmatrix} = \begin{bmatrix} x \\ y \\ z \\ \cdots \\ \phi \\ \theta \\ \psi \end{bmatrix}. \tag{55}$$

This means

$$\dot{Y} = \begin{bmatrix} R_b^e & \mathbf{0} \\ \mathbf{0} & \Psi \end{bmatrix} \begin{bmatrix} \varepsilon \\ \zeta \end{bmatrix} \tag{56}$$

and

$$\ddot{Y} = \begin{bmatrix} \dot{R}_b^e \varepsilon + R_b^e \dot{\varepsilon} \\ \dot{\Psi}\zeta + \Psi\dot{\zeta} \end{bmatrix} = f(Y, \varepsilon, \zeta, \bar{U}). \tag{57}$$

This concludes that the relative degree of the system in compact form is $2 + 2 = 4$ which is equal to the number of state vectors ε, ζ, Y_1 and Y_2, and there is no hidden dynamics. This makes the synthesis of the sliding-mode control possible with no risk of internal instability.

4.2. *Sliding-mode control*

To synthesize the sliding-mode control, we define the absolute displacement error as

$$e = Y - Y_d, \tag{58}$$

with Y_d being the determined target of the absolute position and orientation of the system. It is needless to mention that Y, Y_d and e are functions of time and the argument t is omitted for simplicity of representations. The system is nonlinear with fast dynamics and our goal is to design a state feedback control law such that Y asymptotically tracks the determined trajectory Y_d which means e is bounded and converges to zero.

The absolute velocity error is $\dot{e}$ and the absolute acceleration error is $\ddot{e}$. They can be derived as

$$\dot{e} = \dot{Y} - \dot{Y}_d \tag{59}$$

$$= \begin{bmatrix} R_b^e & \mathbf{0} \\ \mathbf{0} & \Psi \end{bmatrix} \begin{bmatrix} \varepsilon \\ \zeta \end{bmatrix} - \dot{Y}_d \tag{60}$$

and

$$\ddot{e} = \ddot{Y} - \ddot{Y}d \tag{61}$$

$$= \begin{bmatrix} \dot{R}_b^e \varepsilon + R_b^e \dot{\varepsilon} \\ \dot{\Psi}\zeta + \Psi\dot{\zeta} \end{bmatrix} - \ddot{Y}_d \tag{62}$$

$$= \begin{bmatrix} \dot{R}_b^e \varepsilon + R_b^e (N_1 + \bar{U}_1) \\ \dot{\Psi}\zeta + \Psi(N_2 + \bar{U}_2) \end{bmatrix} - \ddot{Y}_d \tag{63}$$

$$= \begin{bmatrix} \dot{R}_b^e \varepsilon + R_b^e N_1 \\ \dot{\Psi}\zeta + \Psi N_2 \end{bmatrix} + \begin{bmatrix} R_b^e & \mathbf{0} \\ \mathbf{0} & \Psi \end{bmatrix} \begin{bmatrix} \bar{U}_1 \\ \bar{U}_2 \end{bmatrix} - \ddot{Y}_d \tag{64}$$

$$= M_1 + M_2 \bar{U} - \ddot{Y}_d, \tag{65}$$

where

$$M_1 = \begin{bmatrix} \dot{R}_b^e \varepsilon + R_b^e N_1 \\ \dot{\Psi}\zeta + \Psi N_2 \end{bmatrix}, \qquad M_2 = \begin{bmatrix} R_b^e & \mathbf{0} \\ \mathbf{0} & \Psi \end{bmatrix} \tag{66}$$

and $\bar{U}$ is as defined in Eq. (38). We assume that Y_d, $\dot{Y}_d$ and $\ddot{Y}_d$ are bounded for all $t > 0$ and they are available online.

We define a set of sliding-mode surfaces as $s = ke + \underline{e}$ with $k > 0$. This gives

$$\dot{s} = k\dot{e} + \ddot{e} \tag{67}$$

$$= k\dot{e} + M_1 + M_2 \bar{U} - \ddot{Y}_d. \tag{68}$$

It is worth mentioning here that s is a vector with the dimension of 6×1. Hence, s is a group of six sliding-mode manifolds with each sliding-mode surface being denoted as s_i, $i \in \{1, 2, \ldots, 6\}$.

To analyze the performance of the designed sliding-mode controller, we examine the reaching phase by using a Lyapunov function defined as $V(s) = \frac{1}{2} s^T s$. We have

$$\dot{V} = s^T \dot{s}. \tag{69}$$

We put

$$\dot{s} = \mathrm{v}, \tag{70}$$

where v is the artificial control input, or the pure switching component, that we choose to define as

$$\mathrm{v} = -\beta_1 s - \beta_2 \mathrm{sign}(s) \qquad \text{with } \beta_1, \beta_2 > 0. \tag{71}$$

Here, $\text{sgn}(s)$ represents the sign function of the sliding surfaces and is defined as

$$\text{sgn}(s) = \begin{bmatrix} \text{sgn}(s_1) \\ \text{sgn}(s_2) \\ \vdots \\ \text{sgn}(s_6) \end{bmatrix}, \quad \text{where } \text{sgn}(s_i) = \begin{cases} +1 & \text{if } s_i > 0, \\ 0 & \text{if } s_i = 0, \\ -1 & \text{if } s_i < 0. \end{cases} \tag{72}$$

This leads to

$$\dot{V} = s^T(-\beta_1 s - \beta_2 \text{sgn}(s)) \tag{73}$$

$$= -\beta_1 s^T s - \beta_2 |s| < 0 \qquad \text{for all } s \neq 0, \tag{74}$$

where $|s|$ is equal to the sum of all elements of the sliding surface $|s| = \Sigma_1^6 |s_i|$. As $\dot{V} < 0$ for all $s \neq 0$, this ensures that all trajectories starting off the manifold $s = 0$ reach it in finite time and those on the manifold cannot leave it.

To compensate for the chattering effect and avoid control discontinuities in the control loop, we define the artificial control input v using the boundary layer solution [45] such as

$$\text{v} = \begin{bmatrix} v_1 \\ v_2 \\ \vdots \\ v_6 \end{bmatrix}, \quad \text{where } \text{v}_i = -\beta_1 s_i - \begin{cases} \beta_2 \text{sgn}(s_i) & \text{when } |s_i| > \epsilon, \\ \dfrac{\beta_2}{\epsilon} \text{sgn}(s_i) & \text{when } |s_i| \leq \epsilon, \end{cases} \tag{75}$$

for all $i \in \{1, 2, \ldots, 6\}$ with ϵ being a small positive value to be chosen by the designer. The value of ϵ represents the range of the boundary layer that is imposed to prevent chattering of the controller. Now, to obtain $\bar{U}$, we can use Eqs. (68) and (70) to get

$$\bar{U} = M_2^{-1}(-M_1 - k\dot{e} + \ddot{Y}_d + v). \tag{76}$$

The stability analysis of the designed sliding-mode controller can be established by considering the error dynamics. We define $\xi_1 = e$ and $\xi_2 = \dot{e}$. This leads to

$$\dot{\xi}_1 = \xi_2, \tag{77}$$

$$\dot{\xi}_2 = M_1 + M_2 \bar{U} - \ddot{Y}_d = -k\xi_2 + v, \tag{78}$$

with the term v defined as in Eq. (75) and $\beta_1, \beta_2 > 0$, so it is straightforward to conclude that there exists a finite time T_1 such that the error is bounded for all $t \geq T_1$. This shows that the derived sliding mode is stable.

4.3. *Determining the speed of BLDC motors and the angles of the servo motors*

After obtaining the control input $\bar{U}$, we can solve the equations set (40)–(46) to obtain the physical quantities of the servo angles and the rotational speed of the brushless DC motors. However, these equations are nonlinear and are computationally expensive to solve. The equations can be rewritten as

$$\bar{U} = AU, \tag{79}$$

with

$$A = \begin{bmatrix} 0 & 0 & 0 & 0 & k_t & 0 & -k_t & 0 \\ k_t & 0 & -k_t & 0 & 0 & 0 & 0 & 0 \\ 0 & k_t & 0 & k_t & 0 & k_t & 0 & k_t \\ 0 & 0 & 0 & 0 & -k_d & -lk_f & -k_d & lk_f \\ -k_d & -lk_f & -k_d & lk_f & 0 & 0 & 0 & 0 \\ lk_f & -k_d & lk_f & k_d & lk_f & -k_d & lk_f & k_d \end{bmatrix}. \tag{80}$$

If we manage to solve Eq. (79) to find U, it will be straightforward to determine the rotational speed of the rotors and tilting angles of the servos from U. However, we have $\bar{U} \in R^{6\times1}$, $U \in R^{8\times1}$ and the matrix $A \in R^{6\times8}$ is not square which presents a computational challenge for any onboard controller. This control problem can be solved by choosing an operating point P_i that results in $U_{P_i} \in R^{6\times1} \subset U$ and makes, based on the analysis of the forces and torques, the matrix $A_{P_i} \in R^{6\times6} \subset A$ square while guaranteeing that $\text{rank}(A_{P_i}) = 6$. For instance, the operating point of ($\alpha_1 = 0$, $\alpha_2 = \frac{\pi}{2}$) can satisfy this condition and make the solution for U possible. Another operating point that can be considered is ($\alpha_3 = 0$, $\alpha_4 = \frac{\pi}{2}$) or any other reasonable operational assumption. This is a switching control technique that enables the controller to determine a solution for the equation $U = A^{-1}\bar{U}$ which leads to the calculation of the rotor speeds and tilting angles from Eq. (9). The only condition that needs to be enforced for any chosen operating point is that $\text{rank}(A_{P_i}) = 6$. For instance, the point ($\alpha_1 = \alpha_2$, $\alpha_3 = \alpha_3$) or ($\omega_1 = \omega_2$, $\omega_3 = \omega_4$) gives an operation point with $\text{rank}(A_{P_i}) = 4$ which makes the matrix A_{P_i} ill-posed and then the solution of Eq. (79) becomes nonunique. Also, for the special case of ($\alpha_1 = -\alpha_2$, $\alpha_3 = -\alpha_4$, $\omega_1 = \omega_2$, $\omega_3 = \omega_4$), we have $U_p = U_q = U_r = 0$. This makes the attitude of the quadrotor uncontrollable and these operating points should be avoided.

Without loss of generality, we can select a limited number of predetermined operating points where the controller can switch between these operating points based on the flight conditions. In this paper, we consider the following four operating points:

$$P_1 : \alpha_3 = \frac{\pi}{2}, \qquad \alpha_4 = 0, \tag{81}$$

$$P_2 : \alpha_3 = 0, \qquad \alpha_4 = \frac{\pi}{2}, \tag{82}$$

$$P_3 : \alpha_1 = \frac{\pi}{2}, \qquad \alpha_2 = 0, \tag{83}$$

$$P_4 : \alpha_1 = 0, \qquad \alpha_2 = \frac{\pi}{2}, \tag{84}$$

where each operating point will result in a new nonsingular matrix $A_{P_i} \subset A$ with $\text{rank}(A_{P_i}) = 6$ for $i = 1, \ldots, 4$. The tilting angle $\alpha_i = \frac{\pi}{2}$ will mainly have impact on the XY-plane. Therefore, the switching between these operating points can be determined by the direction of flight on the XY-plane. This can be regulated by the following algorithm:

$$\begin{aligned} &\text{if } |u| \geq |v| \text{ and } u \geq 0, \\ &\quad \text{the vehicle operates at } P_1 \text{ and we have } U_{P_1} = A_{P_1}^{-1}\bar{U}; \end{aligned} \tag{85}$$

$$\begin{aligned} &\text{if } |u| \geq |v| \text{ and } u < 0, \\ &\quad \text{the vehicle operates at } P_2 \text{ and we have } U_{P_2} = A_{P_2}^{-1}\bar{U}; \end{aligned} \tag{86}$$

$$\begin{aligned} &\text{if } |v| > |u| \text{ and } v > 0, \\ &\quad \text{the vehicle operates at } P_3 \text{ and we have } U_{P_3} = A_{P_3}^{-1}\bar{U}; \end{aligned} \tag{87}$$

$$\begin{aligned} &\text{if } |v| > |u| \text{ and } v < 0, \\ &\quad \text{the vehicle operates at } P_4 \text{ and we have } U_{P_4} = A_{P_4}^{-1}\bar{U}. \end{aligned} \tag{88}$$

The physical interpretation of the above algorithm is that the selection of the operating point will be such as to generate more thrust in the direction of flight in the XY-plane. This will enhance the ability of the UAV to overcome any wind opposing its movement.

For the purpose of illustration, we will consider the operating point P_4 where $\alpha_1 = 0$, $\alpha_2 = \frac{\pi}{2}$. In this case, the physical input vector U_{P_4} can be obtained as

$$U_{P_4} = A_{P_4}^{-1}\bar{U}, \tag{89}$$

where

$$U_{P_4} = \begin{bmatrix} U_1 \\ \vdots \\ U_6 \end{bmatrix} \quad \text{and} \quad A_{P_4} = \begin{bmatrix} 0 & 0 & k_t & 0 & -k_t & 0 \\ 0 & -k_t & 0 & 0 & 0 & 0 \\ k_t & 0 & 0 & k_t & 0 & k_t \\ 0 & 0 & -k_d & -lk_f & -k_d & lk_f \\ -lk_f & -k_d & 0 & 0 & 0 & 0 \\ -k_d & lk_f & lk_f & -k_d & lk_f & k_d \end{bmatrix}. \tag{90}$$

The matrix A_{P_4} is square and nonsingular. It is independent of the position and attitude of the vehicle and therefore its inverse exists always. Then, from Eq. (9), the rotational speed of the rotors can be determined as

$$\omega_1 = \sqrt[4]{U_1^2}, \tag{91}$$

$$\omega_2 = \sqrt[4]{U_2^2}, \tag{92}$$

$$\omega_3 = \sqrt[4]{U_3^2 + U_4^2}, \tag{93}$$

$$\omega_4 = \sqrt[4]{U_5^2 + U_6^2} \tag{94}$$

and the servo angles can be determined as

$$\alpha_3 = \tan^{-1}\left(\frac{U_3}{U_4}\right), \tag{95}$$

$$\alpha_4 = \tan^{-1}\left(\frac{U_5}{U_6}\right). \tag{96}$$

Similar derivation for the other operating points can be obtained easily.

It is important to state here that while the results of this paper are based on the selection of four operating points for the switching-mode control, the designer has the full freedom of choosing any number of operating points. As long as the condition of any selected point, i.e. $\text{rank}(A_{P_i}) = 6$, is fulfilled, the chosen number of operating points should not affect the results and it is just a matter of design preferences based on the specific situation.

5. Simulation Results

In this section, we show some simulation results to demonstrate the proposed control design and the ability of the system. The simulation is conducted in Matlab 2019b and the parameters used to simulate the system are presented in Table 1. These parameters represent realistic values of a small-size lab-based UAV with some payload. The thrust constant and drag constant are calculated for off-the-shelf propellers of suitable size that have been used by the authors in other projects.

The controller is implemented using the tuned parameters of $k = 1$, $\beta_1 = 1.1$, $\beta_2 = 1.1$ and $\epsilon = 0.1$. The selection of these parameters is based on the observation of the actuator load where higher values of k, β_1 and β_2 will create tighter control performances with higher load on the actuators. On the contrary, small values of β_1 and β_2 will

Table 1. Simulation parameters for the UAV system.

Description	Symbol	Value	Unit
Total mass of the UAV	m	2	kg
Arm length	l	0.25	m
Inertia around the X-axis	I_{xx}	0.008	kg·m^2
Inertia around the Y-axis	I_{yy}	0.008	kg·m^2
Inertia around the Z-axis	I_{zz}	0.013	kg·m^2
Thrust constant	k_f	3.13×10^{-5}	kg·m
Drag constant	k_d	7.5×10^{-7}	kg·m^2

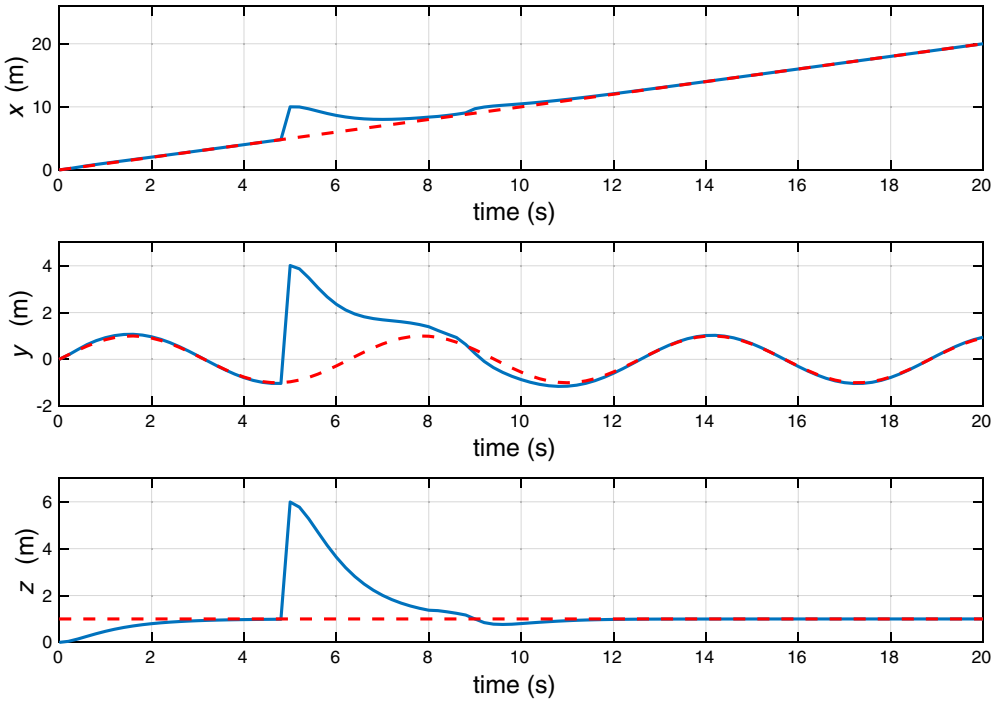

Fig. 6. Position of the UAV for the scenario of flying in a sinusoidal pattern at a fixed altitude under the disturbances. The reference trajectory is in red-dashed line and the actual UAV position is in blue-solid line.

relax the control performance with less load on the actuators. The value of ϵ controls the chattering phenomenon. We need to choose ϵ as small as possible, but a too small value will induce chattering in the presence of unmodeled dynamics or disturbances. Full discussion about the tuning of these parameters and their impact on the sliding control performance is well established in the literature and it is beyond the scope of this paper. More information related to the tuning of these control parameters can be found in [46].

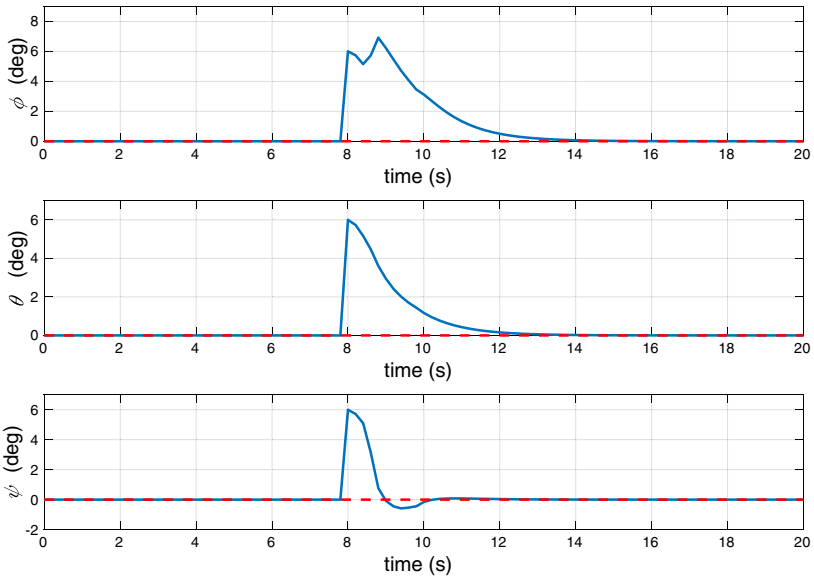

Fig. 7. Orientation of the UAV for the scenario of flying in a sinusoidal pattern at a fixed altitude under the disturbances. The reference trajectory is in red-dashed line and the actual UAV orientation is in blue-solid line.

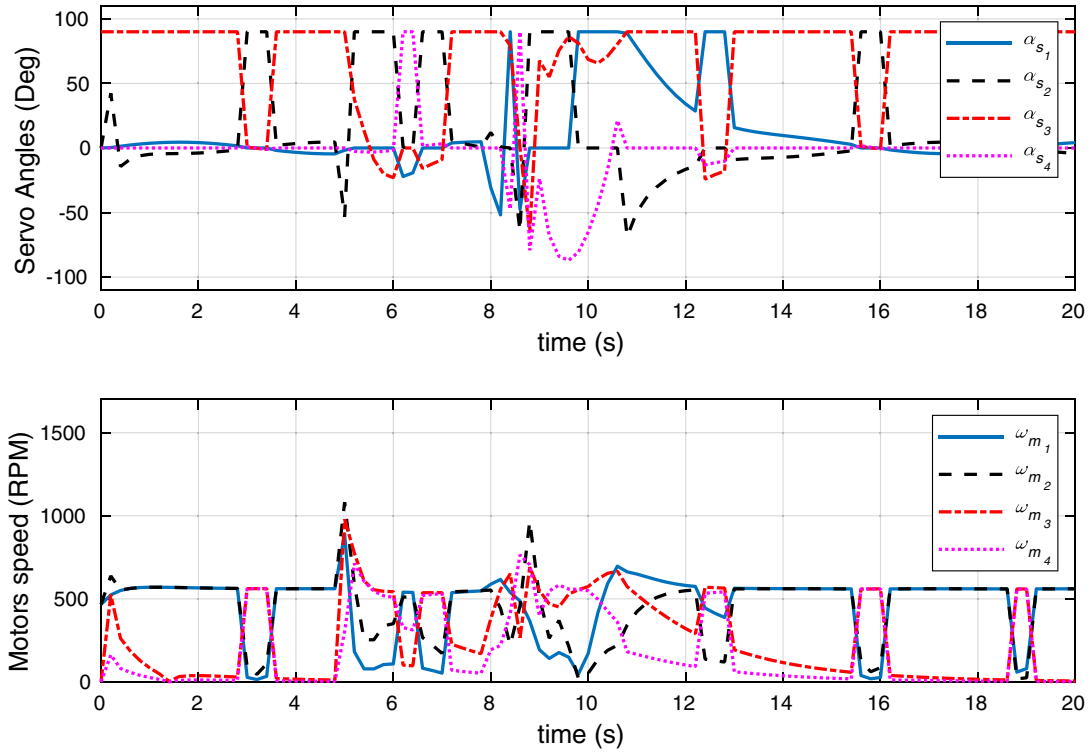

Fig. 8. Actuators' load (angles of servo motors and speed of brushless DC motors) for the scenario of flying in a sinusoidal pattern at a fixed altitude under the disturbances.

We run the simulation for the case of flying in a sinusoidal pattern at a fixed altitude. The flight will be examined under the scenario of normal operation and under the scenario of actuator fault including a faulty rotor or a faulty servo. All flight scenarios are conducted in the presence of disturbances that result from winds which start at a certain point of time during the flight. Attention will be given to the ability of the system to reject disturbances and get back to track while maintaining original orientation of the system even with a faulty actuator. The wind disturbances will take the form of a constant blow that affects the orientation and the position alike. The wind effect can be simulated by a step function of the form

$$D(t) = D_m d(t - t_0), \tag{97}$$

with $D_m \in \mathbb{R}^{3\times 1}$ and $d(t)$ being the unity function. The magnitude of the disturbances is $D_m = [5, 5, 5]^T$ on the position vector and is $D_m = [6, 6, 6]^T$ on the orientation vector. The magnitude of the wind impact is chosen based on the simulation scenario where a disturbance of 5 m on the position vector represents a 500% disturbance on the reference trajectory as the UAV flies at an altitude of 1 m with a sine wave pattern of 1-m magnitude. This represents a huge disturbance impact which highlights the case of harsh and challenging environment. Also, a disturbance magnitude of 6° on the orientation vector represents a strong shift from the set point and it is the limit of the small angle convention that is used in UAV systems. The wind disturbances are simulated to affect the position and orientation of the UAV at different times of $t_0 = 5$ s and

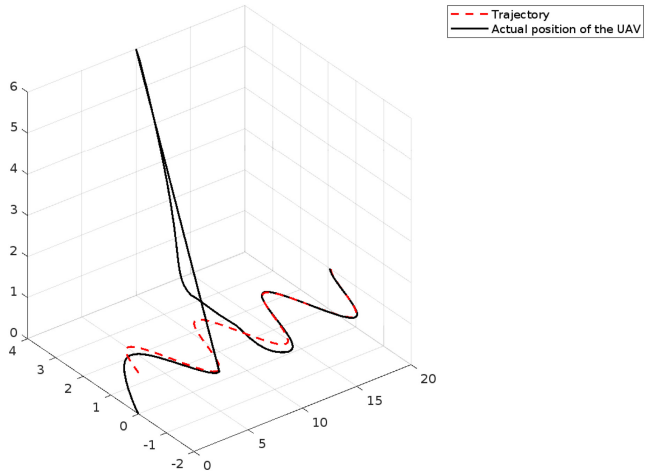

Fig. 9. The 3D flight track for the scenario of flying in a sinusoidal pattern at a fixed altitude under the disturbances. The reference track is in red-dashed line and the actual UAV trajectory is in black-solid line.

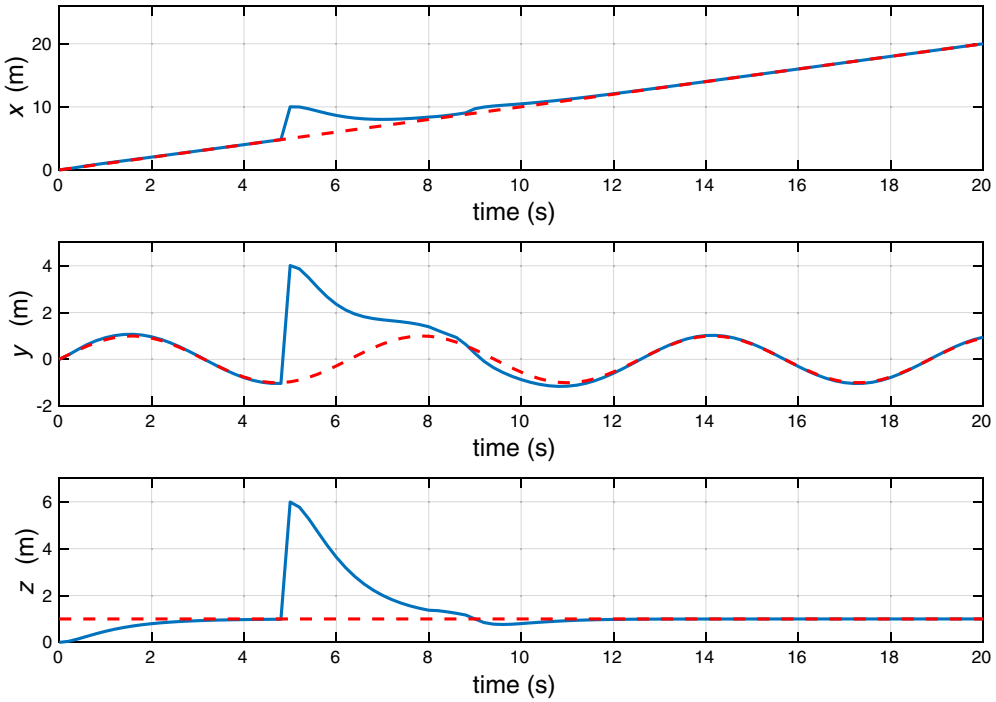

Fig. 10. Position of the UAV for flying in a sinusoidal pattern at a fixed altitude when rotor 1 is faulty and with the disturbances. The reference trajectory is in red-dashed line and the actual UAV position is in blue-solid line.

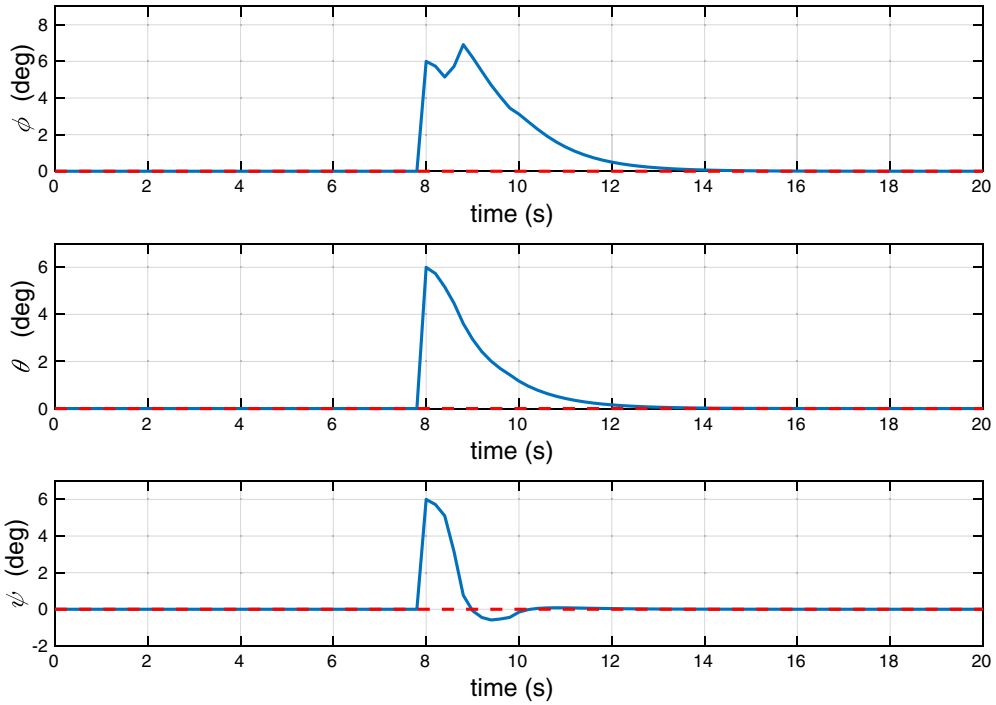

Fig. 11. Orientation of the UAV for flying in a sinusoidal pattern at a fixed altitude when rotor 1 is faulty and with the disturbances. The reference trajectory is in red-dashed line and the actual UAV orientation is in blue-solid line.

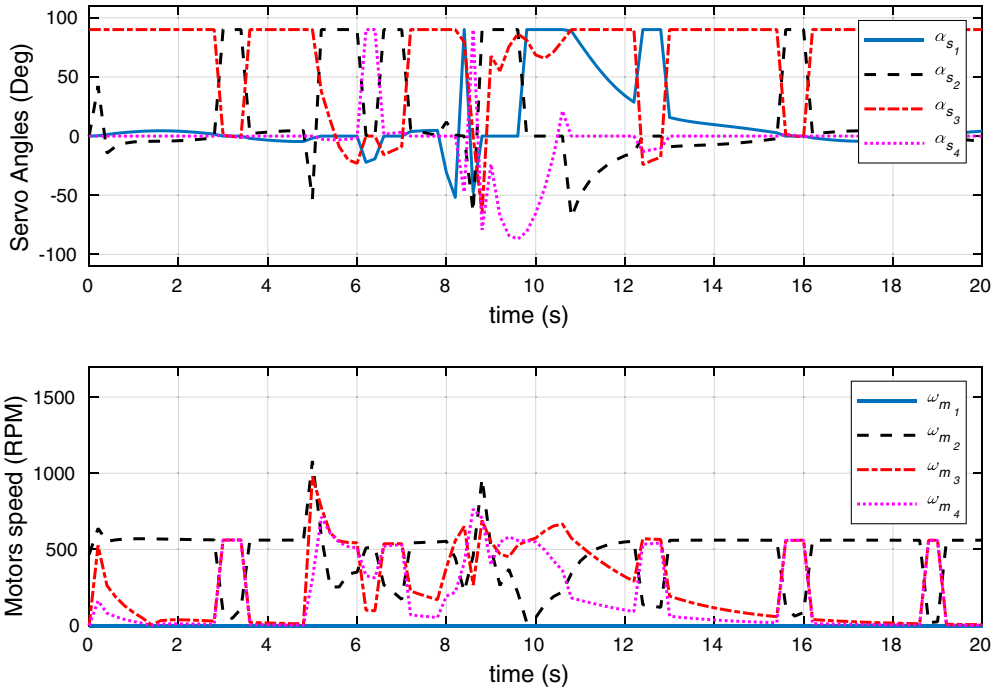

Fig. 12. Actuators' load (angles of servo motors and speed of brushless DC motors) for flying in a sinusoidal pattern at a fixed altitude when rotor 1 is faulty and with the disturbances.

$t_0 = 8$ s, respectively, in order to demonstrate the impact on the actuators for each case separately.

To demonstrate the advantages of the thrust vectoring technique, the flight scenario will be simulated for a reference of fixed orientation at $(0, 0, 0)$. This is to prove that the vehicle can travel to any point in any pattern while maintaining a fixed orientation which is one of the main advantages of the proposed overactuated system. It increases the maneuverability of the vehicle without affecting its orientation which is useful to balance any load the system carries such as a camera.

The simulation of the nominal scenario, under no actuator fault, is demonstrated in Figs. 6 and 7, while the actuators' load is shown in Fig. 8. The 3D flight path is demonstrated in Fig. 9. As it can be seen from these figures, the overactuation design of the system enables the position of the vehicle to change without any tilting which is a unique feature of the system compared with traditional quadrotor configuration. We can see that the controller guarantees tracking, manages to overcome the wind and brings the system back to track. The simulation results show clearly the advantages of the proposed overactuated system with thrust vectoring techniques where the disturbances to the position are rejected without affecting the attitude. Similarly, the disturbances to the attitude are rejected without affecting the position of the vehicle. In the conventional quadrotor systems, this is impossible where the position and attitude of the system are coupled and both will be affected by any wind or external disturbances. The profile of the actuator load indicates that in an ideal case with no disturbances mainly two motors are rotating to generate the required thrust and these are the motors of the same pair that rotate in opposite direction. This mode of

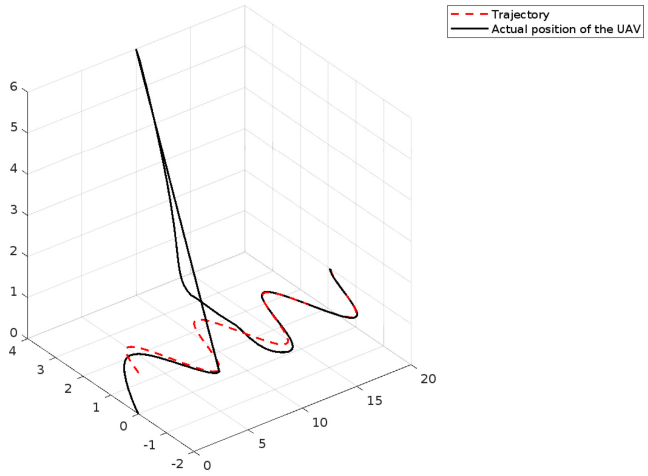

Fig. 13. The 3D flight track for flying in a sinusoidal pattern at a fixed altitude when rotor 1 is faulty and with the disturbances. The reference track is in red-dashed line and the actual UAV trajectory is in black-solid line.

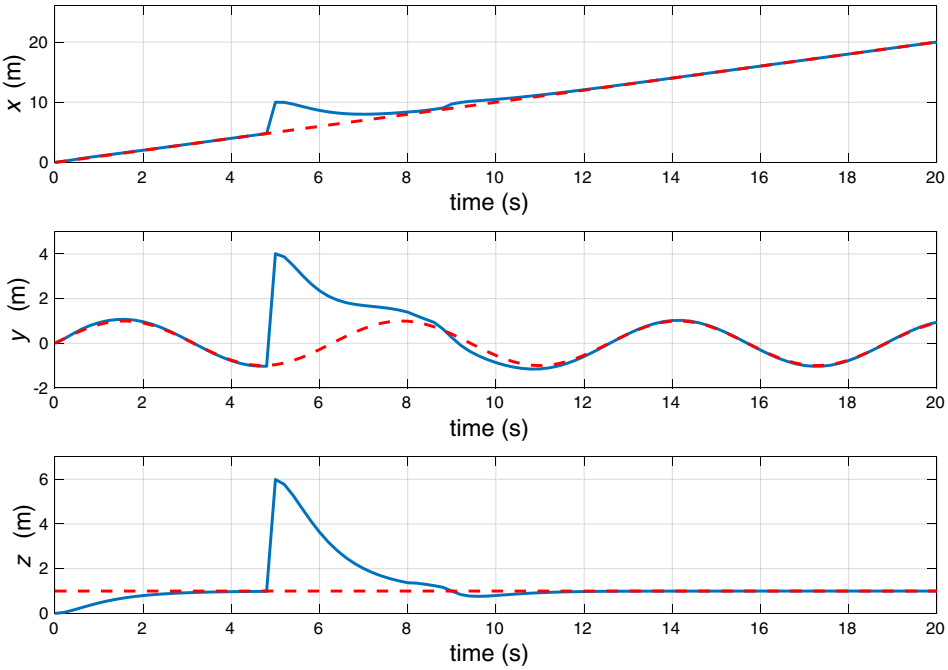

Fig. 14. Position of the UAV for flying in a sinusoidal pattern at a fixed altitude when servo 2 is faulty and with the disturbances. The reference trajectory is in red-dashed line and the actual UAV position is in blue-solid line.

operation can help in extending the time of flight where less energy is required from the battery.

Figures 10–13 show how the vehicle can withstand a faulty rotor and achieve trajectory tracking even under the impact of disturbances. We operate the vehicle under the same flight pattern while rotor 1 is switched off. The results show clearly that even with one of the rotors not working the UAV can still follow the trajectory and reject disturbances.

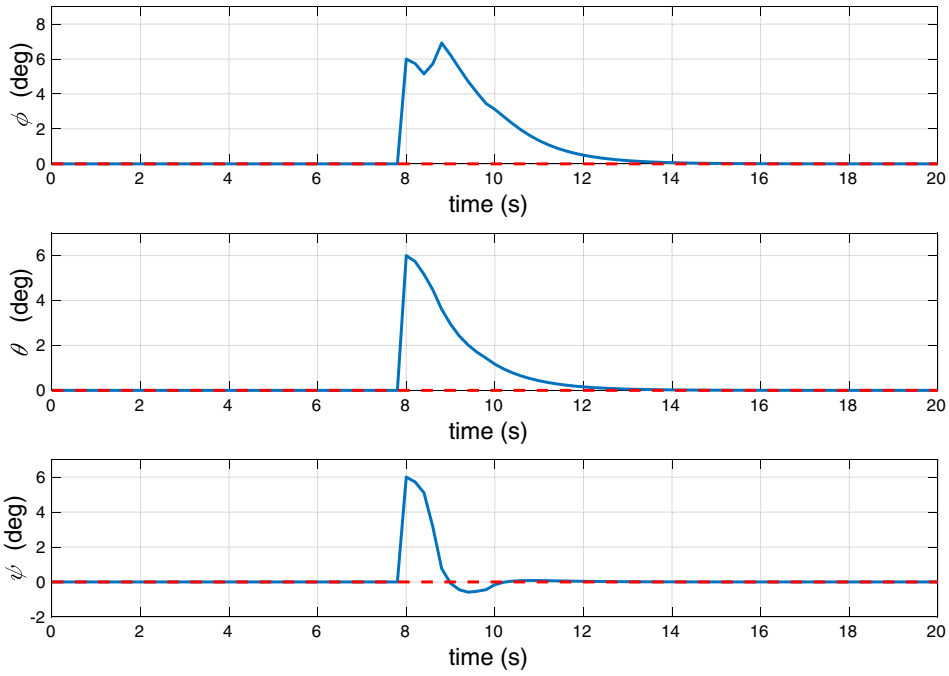

Fig. 15. Orientation of the UAV for flying in a sinusoidal pattern at a fixed altitude when servo 2 is faulty and with the disturbances. The reference trajectory is in red-dashed line and the actual UAV orientation is in blue-solid line.

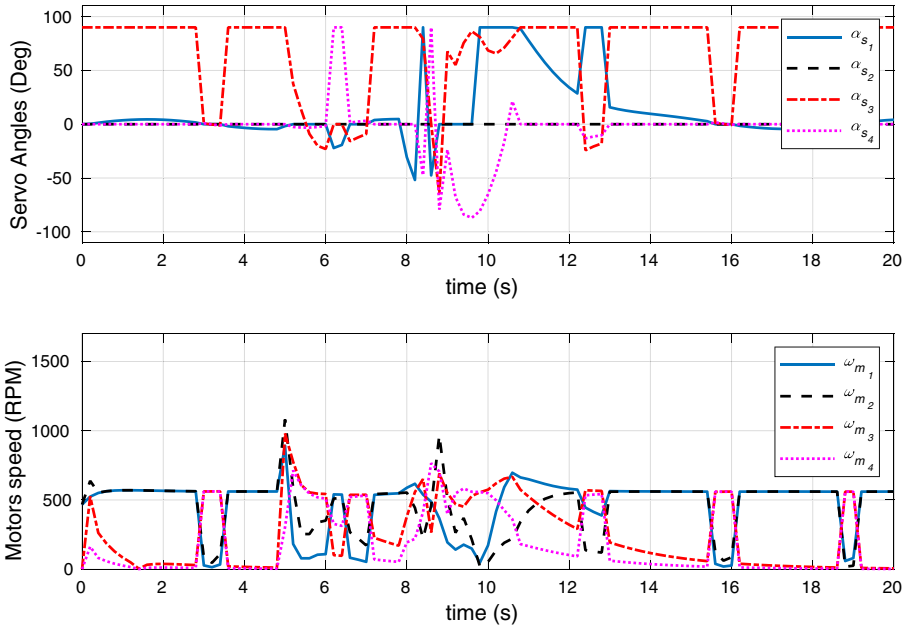

Fig. 16. Actuators' load (angles of servo motors and speed of brushless DC motors) for flying in a sinusoidal pattern at a fixed altitude when servo 2 is faulty and with the disturbances.

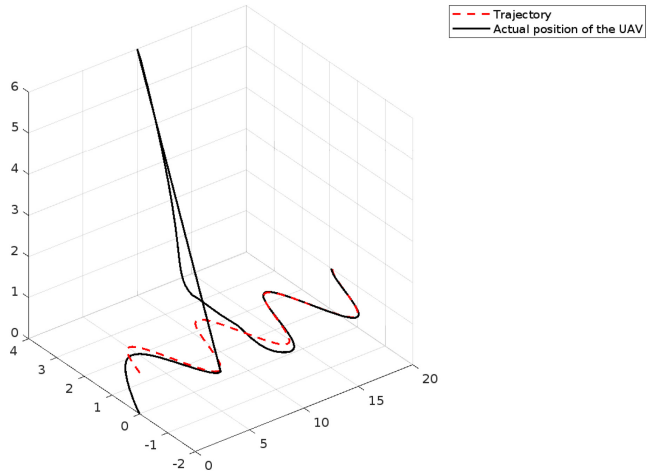

Fig. 17. The 3D flight track for flying in a sinusoidal pattern at a fixed altitude when servo 2 is faulty and with the disturbances. The reference track is in red-dashed line and the actual UAV trajectory is in black-solid line.

Figures 14–17 show how the vehicle can withstand a faulty servo and achieve trajectory tracking even under the impact of disturbances. In this case, servo 2 is turned off and the vehicle is tested for the same flight pattern as above. The results show clearly that even with one of the servos not working the UAV can still follow the trajectory and reject disturbances. The choice of the faulty rotor and servo is random and the results are rigorous regardless of the chosen rotor or servo for the fault tolerance test.

6. Conclusion

This paper proposes an innovative overactuated quadrotor system controlled by a sliding mode associated with switching control algorithm. The UAV has six DoFs with eight actuators where each rotor can tilt independently using a servo motor. The configuration of the system and its proposed control algorithm guarantee decoupling between attitude and position of the vehicle which helps to achieve independent position and orientation references. The system has also strong ability to reject huge disturbances and has good tolerance toward any faulty actuator during the operation which is very advantageous for operating within extreme and challenging environments. Results of this paper are verified in simulation for various scenarios to demonstrate the concept of the vehicle, its ability and the robustness of the proposed control algorithm against large disturbances and actuator fault. Future research will focus on testing the proposed configuration and control algorithm for different UAV sizes with hardware test results.

ORCID

Mohamed Kara-Mohamed https://orcid.org/0000-0001-6423-7275

Qian Zhang https://orcid.org/0000-0002-0651-469X
Xinggang Yan https://orcid.org/0000-0003-2217-8398

References

[1] J. A. Elmore, E. A. Schultz, L. R. Jones, K. O. Evans, S. Samiappan, M. B. Pfeiffer, B. F. Blackwell and R. B. Iglay, Evidence on the efficacy of small unoccupied aircraft systems (UAS) as a survey tool for North American terrestrial, vertebrate animals: a systematic map, *Environ. Evid.* **12**(1) (2023) 3, doi: 10.1186/s13750–022-00294-8.

[2] F. Mechan, Z. Bartonicek, D. Malone and R. S. Lees, Unmanned aerial vehicles for surveillance and control of vectors of malaria and other vector-borne diseases, *Malar. J.* **22**(1) (2023) 23, doi: 10.1186/s12936-022-04414-0.

[3] H. Shakhatreh, A. Sawalmeh, A. Al-Fuqaha, Z. Dou, E. Almaita, I. Khalil, N. S. Othman, A. Khreishah and M. Guizani, Unmanned aerial vehicles: A survey on civil applications and key research challenges, *IEEE Access* **7** (2019) 48572–48634, doi: 10.1109/ACCESS.2019.2909530, arXiv:1805.00881 [cs.RO].

[4] D. Shatat and T. A. Tutunji, UAV quadrotor implementation: A case study, in *Proc. 2014 IEEE 11th Int. Multi-Conf. Systems, Signals & Devices (SSD14)* (IEEE, 2014), pp. 1–6, doi: 10.1109/SSD.2014.6808802.

[5] T. P. Nascimento and M. Saska, Position and attitude control of multi-rotor aerial vehicles: A survey, *Annu. Rev. Control* **48** (2019) 129–146, doi: 10.1016/j.arcontrol.2019.08.004.

[6] H. Shraim, A. Awada and R. Youness, A survey on quadrotors: Configurations, modeling and identification, control, collision avoidance, fault diagnosis and tolerant control, *IEEE Aerosp. Electron. Syst. Mag.* **33**(7) (2018) 14–33, doi: 10.1109/MAES.2018.160246.

[7] A. Bojeri, E. Mai, G. Ristorto, R. Parin, A. Vilardi and G. Guglieri, Characterisation of unmanned aerial vehicle performance under extreme environmental conditions in a controlled atmospheric facility, in *Proc. 2022 Int. Conf. Unmanned Aircraft Systems (ICUAS)* (2022), pp. 1030–1039, doi: 10.1109/ICUAS54217.2022.9836145.

[8] A. J. Wadcock, L. A. Ewing, E. Solis, M. Potsdam and G. Rajagopalan, Rotorcraft downwash flow field study to understand the aerodynamics of helicopter brownout, in *Proc. American Helicopter Society Southwest Region Technical Specialists' Meeting, "Technologies for the Next Generation of Vertical Lift Aircraft"* (2008).

[9] Y. Li, G. Qiao, S. Popov, X. Cui, I. V. Florinsky, X. Yuan and L. Wang, Unmanned aerial vehicle remote sensing for Antarctic research: A review of progress, current applications, and future use cases, *IEEE Geosci. Remote Sens. Mag.* **11**(1) (2023) 73–93, doi: 10.1109/MGRS.2022.3227056.

[10] L. Xu, H. Ma, D. Guo, A.-H. Xie and D.-L. Song, Backstepping sliding-mode and cascade active disturbance rejection control for a quadrotor UAV, *IEEE/ASME Trans. Mechatron.* **25** (2020) 2743–2753, doi: 10.1109/TMECH.2020.2990582.

[11] J. Yang, C. Liu, M. Coombes, Y. Yan and W.-H. Chen, Optimal path following for small fixed-wing UAVs under wind disturbances, *IEEE Trans. Control Syst. Technol.* **29** (2021) 996–1008, doi: 10.1109/TCST.2020.2980727.

[12] R. Zhang, Q. Quan and K.-Y. Cai, Attitude control of a quadrotor aircraft subject to a class of time-varying disturbances, *IET Control Theory Appl.* **5**(9) (2011) 1140–1146, doi: 10.1049/iet-cta.2010.0273.

[13] M. K. Joyo, D. Hazry, S. Faiz Ahmed, M. H. Tanveer, F. A. Warsi and A. T. Hussain, Altitude and horizontal motion control of quadrotor UAV in the presence of air turbulence, in *Proc. 2013 IEEE Conf. Systems, Process & Control (ICSPC)* (IEEE, 2013), pp. 16–20, doi: 10.1109/SPC.2013.6735095.

[14] L. Derafa, A. Benallegue and L. Fridman, Super twisting control algorithm for the attitude tracking of a four rotors UAV, *J. Frankl. Inst.* **349**(2) (2012) 685–699, doi: 10.1016/j.jfranklin.2011.10.011.

[15] S. Darvishpoor, J. Roshanian and M. Tayefi, A novel concept of VTOL bi-rotor UAV based on moving mass control, *Aerosp. Sci. Technol.* **107** (2020) 106238, doi: 10.1016/j.ast.2020.106238.

[16] H. Xiong, J. Hu and X. Diao, Optimize energy efficiency of quadrotors via arm rotation, *J. Dyn. Syst. Meas. Control* **141**(9) (2019) 091002, doi: 10.1115/1.4043227.

[17] S. Driessens and P. E. I. Pounds, Towards a more efficient quadrotor configuration, in *Proc. 2013 IEEE/RSJ Int. Conf. Intelligent Robots and Systems* (IEEE, 2013), pp. 1386–1392, doi: 10.1109/IROS.2013.6696530.

[18] P. Foehn, D. Falanga, N. Kuppuswamy, R. Tedrake and D. Scaramuzza, Fast trajectory optimization for agile quadrotor maneuvers with a cable-suspended payload, in *Proc. Robotics: Science and Systems* (2017), pp. 1–8, doi: 10.5167/UZH-138923.

[19] C. Zeng, R. Abnous, K. Gabani, S. Chowdhury and V. Maldonado, A new tilt-arm transitioning unmanned aerial vehicle: Introduction and conceptual design, *Aerosp. Sci. Technol.* **99** (2020) 105755, doi: 10.1016/j.ast.2020.105755.

[20] A. Maqsood and T. H. Go, Optimization of transition maneuvers through aerodynamic vectoring, *Aerosp. Sci. Technol.* **23**(1) (2012) 363–371, doi: 10.1016/j.ast.2011.09.004.

[21] B. W. Jiang, C. H. Kuo, K. J. Peng, K. C. Peng, S. H. Hsiung and C. M. Kuo, Thrust vectoring control for infrastructure inspection multirotor vehicle, in *Proc. 2019 IEEE 6th Int. Conf. Industrial Engineering and Applications (ICIEA)* (IEEE, 2019), pp. 209–213, doi: 10.1109/IEA.2019.8714892.

[22] S. Rajappa, M. Ryll, H. H. Bulthoff and A. Franchi, Modeling, control and design optimization for a fully-actuated hexarotor aerial vehicle with tilted propellers, in *Proc. 2015 IEEE Int. Conf. Robotics and Automation (ICRA)* (IEEE, 2015), pp. 4006–4013, doi: 10.1109/ICRA.2015.7139759.

[23] M. Kamel, S. Verling, O. Elkhatib, C. Sprecher, P. Wulkop, Z. Taylor, R. Siegwart and I. Gilitschenski, The Voliro omniorientational hexacopter: An agile and maneuverable tiltable-rotor aerial vehicle, *IEEE Robot. Autom. Mag.* **25**(4) (2018) 34–44, doi: 10.1109/MRA.2018.2866758.

[24] D. Invernizzi and M. Lovera, Trajectory tracking control of thrust-vectoring UAVs, *Automatica* **95** (2018) 180–186, doi: 10.1016/j.automatica.2018.05.024.

[25] M. K. Mohamed and A. Lanzon, Design and control of novel tri-rotor UAV, in *Proc. 2012 UKACC Int. Conf. Control* (IEEE, 2012), pp. 304–309, doi: 10.1109/CONTROL.2012.6334647.

[26] M. Ryll, H. H. Bulthoff and P. R. Giordano, A novel overactuated quadrotor unmanned aerial vehicle: Modeling, control, and experimental validation, *IEEE Trans. Control Syst. Technol.* **23**(2) (2015) 540–556, doi: 10.1109/TCST.2014.2330999.

[27] M.-D. Hua, T. Hamel, P. Morin and C. Samson, Control of VTOL vehicles with thrust-tilting augmentation, *Automatica* **52** (2015) 1–7, doi: 10.1016/j.automatica.2014.10.129.

[28] X. Olaz, D. Alaez, M. Prieto, J. Villadangos and J. J. Astrain, Quadcopter neural controller for take-off and landing in windy environments, *Expert Syst. Appl.* **225** (2023) 120146, doi: 10.1016/j.eswa.2023.120146.

[29] I. H. Imran, A. Can, R. Stolkin and A. Montazeri, Real-time nonlinear parameter estimation and tracking control of unmanned aerial vehicles in closed-loop, *Sci. Rep.* **13**(1) (2023) 3125, doi: 10.1038/s41598-023-29544-6.

[30] O. A. Jasim and S. M. Veres, A robust controller for multi rotor UAVs, *Aerosp. Sci. Technol.* **105** (2020) 106010, doi: 10.1016/j.ast.2020.106010.

[31] S. Jia and J. Shan, Continuous integral sliding mode control for space manipulator with actuator uncertainties, *Aerosp. Sci. Technol.* **106** (2020) 106192, doi: 10.1016/j.ast.2020.106192.

[32] V. I. Utkin, *Sliding Modes in Control and Optimization*, Communications and Control Engineering Series (Springer, Berlin, 1992).

[33] S. Bouabdallah and R. Siegwart, Backstepping and sliding-mode techniques applied to an indoor micro quadrotor, in *Proc. 2005 IEEE Int. Conf. Robotics and Automation* (IEEE, 2005), pp. 2247–2252, doi: 10.1109/ROBOT.2005.1570447.

[34] M. Onder Efe, Robust low altitude behavior control of a quadrotor rotorcraft through sliding modes, in *Proc. 2007 Mediterranean Conf. Control & Automation* (IEEE, 2007), pp. 1–6, doi: 10.1109/MED.2007.4433755.

[35] L. Besnard, Y. B. Shtessel and B. Landrum, Quadrotor vehicle control via sliding mode controller driven by sliding mode disturbance observer, *J. Frankl. Inst.* **349**(2) (2012) 658–684, doi: 10.1016/j.jfranklin.2011.06.031.

[36] M. E. Antonio-Toledo, E. N. Sanchez, A. Y. Alanis, J. Flórez and M. A. Perez-Cisneros, Real-time integral backstepping with sliding mode control for a quadrotor UAV, *IFAC-PapersOnLine* **51**(13) (2018) 549–554, doi: 10.1016/j.ifacol.2018.07.337.

[37] O. Mofid and S. Mobayen, Adaptive finite-time backstepping global sliding mode tracker of quad-rotor UAVs under model uncertainty, wind perturbation, and input saturation, *IEEE Trans. Aerosp. Electron. Syst.* **58**(1) (2022) 140–151, doi: 10.1109/TAES.2021.3098168.

[38] O. Mofid, S. Mobayen and W.-K. Wong, Adaptive terminal sliding mode control for attitude and position tracking control of quadrotor UAVs in the existence of external disturbance, *IEEE Access* **9** (2021) 3428–3440, doi: 10.1109/ACCESS.2020.3047659.

[39] Q. Wang, A. Namiki, A. Asignacion, Z. Li and S. Suzuki, Chattering reduction of sliding mode control for quadrotor UAVs based on reinforcement learning, *Drones* **7**(7) (2023) 420, doi: 10.3390/drones7070420.

[40] V. Utkin and H. Lee, Chattering problem in sliding mode control systems, *IFAC Proc. Vol.* **39**(5) (2006) 1, doi: 10.3182/20060607-3-IT-3902.00003.

[41] H. Lee and V. I. Utkin, Chattering suppression methods in sliding mode control systems, *Annu. Rev. Control* **31**(2) (2007) 179–188, doi: 10.1016/j.arcontrol.2007.08.001.

[42] C. P. E. Y. Huanca, G. P. Incremona and P. Colaneri, Design of a distributed switching model predictive control for quadrotor UAVs aggregation, *IEEE Control Syst. Lett.* **7** (2023) 2964–2969, doi: 10.1109/LCSYS.2023.3291664.

[43] N. Cheng and C. Wang, A switching mode control scheme for the hovering control of quadrotor unmanned aerial vehicles, *Mathematics* **11**(4) (2023) 994, doi: 10.3390/math11040994.

[44] H. Zhang, Y. He and G. Xu, Research on transition process of vertical take-off and landing UAV based on limited time switching control, in *Proc. 2021 IEEE 5th Information Technology, Networking, Electronic and Automation Control Conf. (ITNEC)*, Vol. 5 (2021), pp. 127–131, doi: 10.1109/ITNEC52019.2021.9587122.

[45] V. Utkin and H. Lee, Chattering problem in sliding mode control systems, in *Proc. Int. Workshop on Variable Structure Systems, 2006 (VSS'06)* (IEEE, 2006), pp. 346–350, doi: 10.1109/VSS.2006.1644542.

[46] H. Khalil, *Nonlinear Control: Always Learning* (Pearson Education, 2014).

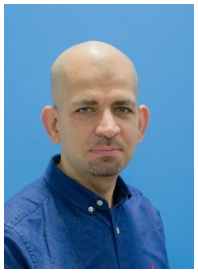

Mohamed Kara-Mohamed is currently a Senior Lecturer in Robotics at Liverpool John Moores University, UK. He holds a PhD degree in Control Engineering from The University of Manchester, UK. His main research interest is within the control and applications of advanced systems including autonomous robotic systems.

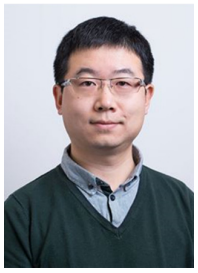

Qian Zhang received the B.Eng. degree in automatic control from Zhejiang University, Zhejiang, China, in 2003, and the Ph.D. degree from the University of Sheffield, U.K., in 2008. He is currently a Reader in Intelligent Systems in the School of Engineering at Liverpool John Moores University (LJMU). His research interests include data-driven modelling, multi-objective optimal design, robotics and control, and their applications in engineering and transport systems.

Xing-Gang Yan received the B.Sc. Degree from Shaanxi Normal University, in 1985, the M.Sc. Degree from Qufu Normal University in 1991, and the Ph.D. Degree of Engineering from Northeastern University, China in 1997. Currently, he is Associate Professor of Control Engineering at the University of Kent, United Kingdom. He worked as a Research Fellow/Research Associate in the Northwestern Polytechnical University, and the University of Hong Kong, China, Nanyang Technological University, Singapore and the University of Leicester, United Kingdom. He was a Lecturer in Qingdao University, China from 1991 to 1994. He is an IEEE member, IET member, HEA Fellow and a Charted Engineer. He received the Best Application Paper Award of ASian Control Conference (ASCC) in Fukuoka, Japan in 2019, and the Outstanding Editor-in-Chief from Bilingual Publishing Group in 2022. He serves as the member of the Editorial Board of several engineering journals including IET Control Theory and Applications, Journal of Franklin Institute, Complexity and Energies etc., and the member of TPC for a number of international conferences. He has published three books, six invited book chapters and over 200 referred papers in the area of control engineering. His research interests including sliding mode control, decentralised control, fault detection and isolation, and time delay systems with applications.